arXiv:hep-ex/9507001v1 5 Jul 1995

Exclusive ρ^0 production in deep inelastic electron-proton scattering at HERA

ZEUS Collaboration

Abstract

The exclusive production of ρ^0 mesons in deep inelastic electron-proton scattering has been studied using the ZEUS detector. Cross sections have been measured in the range $7 < Q^2 < 25$ GeV^2 for γ^*p centre of mass (c.m.) energies from 40 to 130 GeV. The $\gamma^*p \to \rho^0 p$ cross section exhibits a $Q^{-(4.2\pm0.8^{+1.4}_{-0.5})}$ dependence and both longitudinally and transversely polarised ρ^0's are observed. The $\gamma^*p \to \rho^0 p$ cross section rises strongly with increasing c.m. energy, when compared with NMC data at lower energy, which cannot be explained by production through soft pomeron exchange. The data are compared with perturbative QCD calculations where the rise in the cross section reflects the increase in the gluon density at low x. the gluon density at low x.

The ZEUS Collaboration

M. Derrick, D. Krakauer, S. Magill, D. Mikunas, B. Musgrave, J. Repond, R. Stanek, R.L. Talaga, H. Zhang
Argonne National Laboratory, Argonne, IL, USA [p]

R. Ayad[1], G. Bari, M. Basile, L. Bellagamba, D. Boscherini, A. Bruni, G. Bruni, P. Bruni, G. Cara Romeo,
G. Castellini[2], M. Chiarini, L. Cifarelli[3], F. Cindolo, A. Contin, M. Corradi, I. Gialas[4], P. Giusti, G. Iacobucci,
G. Laurenti, G. Levi, A. Margotti, T. Massam, R. Nania, C. Nemoz,
F. Palmonari, A. Polini, G. Sartorelli, R. Timellini, Y. Zamora Garcia[1], A. Zichichi
University and INFN Bologna, Bologna, Italy [f]

A. Bargende[5], J. Crittenden, K. Desch, B. Diekmann[6], T. Doeker, M. Eckert, L. Feld, A. Frey, M. Geerts,
M. Grothe, H. Hartmann, K. Heinloth, E. Hilger, H.-P. Jakob, U.F. Katz, S.M. Mari[4], S. Mengel, J. Mollen,
E. Paul, M. Pfeiffer, Ch. Rembser, D. Schramm, J. Stamm, R. Wedemeyer
Physikalisches Institut der Universität Bonn, Bonn, Federal Republic of Germany [c]

S. Campbell-Robson, A. Cassidy, N. Dyce, B. Foster, S. George, R. Gilmore, G.P. Heath, H.F. Heath, T.J. Llewellyn,
C.J.S. Morgado, D.J.P. Norman, J.A. O'Mara, R.J. Tapper, S.S. Wilson, R. Yoshida
H.H. Wills Physics Laboratory, University of Bristol, Bristol, U.K. [o]

R.R. Rau
Brookhaven National Laboratory, Upton, L.I., USA [p]

M. Arneodo[7], M. Capua, A. Garfagnini, L. Iannotti, M. Schioppa, G. Susinno
Calabria University, Physics Dept.and INFN, Cosenza, Italy [f]

A. Bernstein, A. Caldwell, N. Cartiglia, J.A. Parsons, S. Ritz[8], F. Sciulli, P.B. Straub, L. Wai, S. Yang, Q. Zhu
Columbia University, Nevis Labs., Irvington on Hudson, N.Y., USA [q]

P. Borzemski, J. Chwastowski, A. Eskreys, K. Piotrzkowski, M. Zachara, L. Zawiejski
Inst. of Nuclear Physics, Cracow, Poland [j]

L. Adamczyk, B. Bednarek, K. Jeleń, D. Kisielewska, T. Kowalski, E. Rulikowska-Zarębska,
L. Suszycki, J. Zając
Faculty of Physics and Nuclear Techniques, Academy of Mining and Metallurgy, Cracow, Poland [j]

A. Kotański, M. Przybycień
Jagellonian Univ., Dept. of Physics, Cracow, Poland [k]

L.A.T. Bauerdick, U. Behrens, H. Beier[9], J.K. Bienlein, C. Coldewey, O. Deppe, K. Desler, G. Drews,
M. Flasiński[10], D.J. Gilkinson, C. Glasman, P. Göttlicher, J. Große-Knetter, B. Gutjahr[11], T. Haas, W. Hain,
D. Hasell, H. Heßling, Y. Iga, K. Johnson[12], P. Joos, M. Kasemann, R. Klanner, W. Koch, L. Köpke[13], U. Kötz,
H. Kowalski, J. Labs, A. Ladage, B. Löhr, M. Löwe, D. Lüke, J. Mainusch, O. Mańczak, T. Monteiro[14],
J.S.T. Ng, S. Nickel[15], D. Notz, K. Ohrenberg, M. Roco, M. Rohde, J. Roldán, U. Schneekloth, W. Schulz,
F. Selonke, E. Stiliaris[16], B. Surrow, T. Voß, D. Westphal, G. Wolf, C. Youngman, W. Zeuner, J.F. Zhou[17]
Deutsches Elektronen-Synchrotron DESY, Hamburg, Federal Republic of Germany

H.J. Grabosch, A. Kharchilava, A. Leich, M.C.K. Mattingly, A. Meyer, S. Schlenstedt, N. Wulff
DESY-Zeuthen, Inst. für Hochenergiephysik, Zeuthen, Federal Republic of Germany

G. Barbagli, P. Pelfer
University and INFN, Florence, Italy [f]

G. Anzivino, G. Maccarrone, S. De Pasquale, L. Votano
INFN, Laboratori Nazionali di Frascati, Frascati, Italy [f]

A. Bamberger, S. Eisenhardt, A. Freidhof, S. Söldner-Rembold[18], J. Schroeder[19], T. Trefzger
Fakultät für Physik der Universität Freiburg i.Br., Freiburg i.Br., Federal Republic of Germany [c]

I

N.H. Brook, P.J. Bussey, A.T. Doyle[20], J.I. Fleck[4], D.H. Saxon, M.L. Utley, A.S. Wilson
Dept. of Physics and Astronomy, University of Glasgow, Glasgow, U.K. [o]

A. Dannemann, U. Holm, D. Horstmann, T. Neumann, R. Sinkus, K. Wick
Hamburg University, I. Institute of Exp. Physics, Hamburg, Federal Republic of Germany [c]

E. Badura[21], B.D. Burow[22], L. Hagge, E. Lohrmann, J. Milewski, M. Nakahata[23], N. Pavel, G. Poelz, W. Schott,
F. Zetsche
Hamburg University, II. Institute of Exp. Physics, Hamburg, Federal Republic of Germany [c]

T.C. Bacon, N. Bruemmer, I. Butterworth, E. Gallo, V.L. Harris, B.Y.H. Hung, K.R. Long, D.B. Miller,
P.P.O. Morawitz, A. Prinias, J.K. Sedgbeer, A.F. Whitfield
Imperial College London, High Energy Nuclear Physics Group, London, U.K. [o]

U. Mallik, E. McCliment, M.Z. Wang, S.M. Wang, J.T. Wu
University of Iowa, Physics and Astronomy Dept., Iowa City, USA [p]

P. Cloth, D. Filges
Forschungszentrum Jülich, Institut für Kernphysik, Jülich, Federal Republic of Germany

S.H. An, S.M. Hong, S.W. Nam, S.K. Park, M.H. Suh, S.H. Yon
Korea University, Seoul, Korea [h]

R. Imlay, S. Kartik, H.-J. Kim, R.R. McNeil, W. Metcalf, V.K. Nadendla
Louisiana State University, Dept. of Physics and Astronomy, Baton Rouge, LA, USA [p]

F. Barreiro[24], G. Cases, J.P. Fernandez, R. Graciani, J.M. Hernández, L. Hervás[24], L. Labarga[24], M. Martinez,
J. del Peso, J. Puga, J. Terron, J.F. de Trocóniz
Univer. Autónoma Madrid, Depto de Física Teoríca, Madrid, Spain [n]

G.R. Smith
University of Manitoba, Dept. of Physics, Winnipeg, Manitoba, Canada [a]

F. Corriveau, D.S. Hanna, J. Hartmann, L.W. Hung, J.N. Lim, C.G. Matthews, P.M. Patel,
L.E. Sinclair, D.G. Stairs, M. St.Laurent, R. Ullmann, G. Zacek
McGill University, Dept. of Physics, Montréal, Québec, Canada [a, b]

V. Bashkirov, B.A. Dolgoshein, A. Stifutkin
Moscow Engineering Physics Institute, Mosocw, Russia [l]

G.L. Bashindzhagyan, P.F. Ermolov, L.K. Gladilin, Yu.A. Golubkov, V.D. Kobrin, I.A. Korzhavina, V.A. Kuzmin,
O.Yu. Lukina, A.S. Proskuryakov, A.A. Savin, L.M. Shcheglova, A.N. Solomin,
N.P. Zotov
Moscow State University, Institute of Nuclear Physics, Moscow, Russia [m]

M. Botje, F. Chlebana, A. Dake, J. Engelen, M. de Kamps, P. Kooijman, A. Kruse, H. Tiecke, W. Verkerke,
M. Vreeswijk, L. Wiggers, E. de Wolf, R. van Woudenberg
NIKHEF and University of Amsterdam, Netherlands [i]

D. Acosta, B. Bylsma, L.S. Durkin, K. Honscheid, C. Li, T.Y. Ling, K.W. McLean[25], W.N. Murray, I.H. Park,
T.A. Romanowski[26], R. Seidlein[27]
Ohio State University, Physics Department, Columbus, Ohio, USA [p]

D.S. Bailey, A. Byrne[28], R.J. Cashmore, A.M. Cooper-Sarkar, R.C.E. Devenish, N. Harnew,
M. Lancaster, L. Lindemann[4], J.D. McFall, C. Nath, V.A. Noyes, A. Quadt, J.R. Tickner,
H. Uijterwaal, R. Walczak, D.S. Waters, F.F. Wilson, T. Yip
Department of Physics, University of Oxford, Oxford, U.K. [o]

G. Abbiendi, A. Bertolin, R. Brugnera, R. Carlin, F. Dal Corso, M. De Giorgi, U. Dosselli,
S. Limentani, M. Morandin, M. Posocco, L. Stanco, R. Stroili, C. Voci
Dipartimento di Fisica dell' Universita and INFN, Padova, Italy [f]

II

J. Bulmahn, J.M. Butterworth, R.G. Feild, B.Y. Oh, J.J. Whitmore[29]
Pennsylvania State University, Dept. of Physics, University Park, PA, USA [q]

G. D'Agostini, G. Marini, A. Nigro, E. Tassi
Dipartimento di Fisica, Univ. 'La Sapienza' and INFN, Rome, Italy [f]

J.C. Hart, N.A. McCubbin, K. Prytz, T.P. Shah, T.L. Short
Rutherford Appleton Laboratory, Chilton, Didcot, Oxon, U.K. [o]

E. Barberis, T. Dubbs, C. Heusch, M. Van Hook, W. Lockman, J.T. Rahn, H.F.-W. Sadrozinski, A. Seiden, D.C. Williams
University of California, Santa Cruz, CA, USA [p]

J. Biltzinger, R.J. Seifert, O. Schwarzer, A.H. Walenta, G. Zech
Fachbereich Physik der Universität-Gesamthochschule Siegen, Federal Republic of Germany [c]

H. Abramowicz, G. Briskin, S. Dagan[30], A. Levy[31]
School of Physics,Tel-Aviv University, Tel Aviv, Israel [e]

T. Hasegawa, M. Hazumi, T. Ishii, M. Kuze, S. Mine, Y. Nagasawa, M. Nakao, I. Suzuki, K. Tokushuku, S. Yamada, Y. Yamazaki
Institute for Nuclear Study, University of Tokyo, Tokyo, Japan [g]

M. Chiba, R. Hamatsu, T. Hirose, K. Homma, S. Kitamura, Y. Nakamitsu, K. Yamauchi
Tokyo Metropolitan University, Dept. of Physics, Tokyo, Japan [g]

R. Cirio, M. Costa, M.I. Ferrero, L. Lamberti, S. Maselli, C. Peroni, R. Sacchi, A. Solano, A. Staiano
Universita di Torino, Dipartimento di Fisica Sperimentale and INFN, Torino, Italy [f]

M. Dardo
II Faculty of Sciences, Torino University and INFN - Alessandria, Italy [f]

D.C. Bailey, D. Bandyopadhyay, F. Benard, M. Brkic, D.M. Gingrich[32], G.F. Hartner, K.K. Joo, G.M. Levman, J.F. Martin, R.S. Orr, S. Polenz, C.R. Sampson, R.J. Teuscher
University of Toronto, Dept. of Physics, Toronto, Ont., Canada [a]

C.D. Catterall, T.W. Jones, P.B. Kaziewicz, J.B. Lane, R.L. Saunders, J. Shulman
University College London, Physics and Astronomy Dept., London, U.K. [o]

K. Blankenship, B. Lu, L.W. Mo
Virginia Polytechnic Inst. and State University, Physics Dept., Blacksburg, VA, USA [q]

W. Bogusz, K. Charchuła, J. Ciborowski, J. Gajewski, G. Grzelak, M. Kasprzak, M. Krzyżanowski, K. Muchorowski, R.J. Nowak, J.M. Pawlak, T. Tymieniecka, A.K. Wróblewski, J.A. Zakrzewski, A.F. Żarnecki
Warsaw University, Institute of Experimental Physics, Warsaw, Poland [j]

M. Adamus
Institute for Nuclear Studies, Warsaw, Poland [j]

Y. Eisenberg[30], U. Karshon[30], D. Revel[30], D. Zer-Zion
Weizmann Institute, Nuclear Physics Dept., Rehovot, Israel [d]

I. Ali, W.F. Badgett, B. Behrens, S. Dasu, C. Fordham, C. Foudas, A. Goussiou, R.J. Loveless, D.D. Reeder, S. Silverstein, W.H. Smith, A. Vaiciulis, M. Wodarczyk
University of Wisconsin, Dept. of Physics, Madison, WI, USA [p]

T. Tsurugai
Meiji Gakuin University, Faculty of General Education, Yokohama, Japan

S. Bhadra, M.L. Cardy, C.-P. Fagerstroem, W.R. Frisken, K.M. Furutani, M. Khakzad, W.B. Schmidke
York University, Dept. of Physics, North York, Ont., Canada [a]

1 Introduction

With the high energy electron-proton collider HERA, it has become possible to study deep inelastic scattering (DIS) processes at large values of Q^2, the negative of the four-momentum transfer squared of the exchanged virtual photon, and large values of W, the virtual photon-proton centre of mass (c.m.) energy. The exclusive production of vector mesons in DIS is of particular interest. While numerous data exist at low Q^2 [1-5] on the exclusive reaction

$$e \ (or \ \mu) \ + \ p \rightarrow e \ (or \ \mu) \ + \ \rho^0 \ + p, \tag{1}$$

only two experiments have reported DIS measurements for $Q^2 > 5$ GeV^2 [6, 7]. These latter measurements have been restricted to $W < 20$ GeV.

Previous studies of exclusive leptoproduction ($\gamma^* N \rightarrow \rho^0 N$) and real photoproduction ($\gamma N \rightarrow \rho^0 N$) off a nucleon N have shown that for ρ^0 production at low Q^2 (typically < 2 GeV^2):

- the Q^2 dependence of the cross section can be described by the Vector Dominance Model (VDM) [1] in which it is assumed that the photon fluctuates into a ρ^0 meson yielding:

$$\frac{d\sigma(Q^2)}{dt} = \frac{d\sigma(0)}{dt} \left(\frac{M_\rho^2}{M_\rho^2 + Q^2} \right)^2 \left(1 + \epsilon \xi^2 \frac{Q^2}{M_\rho^2} \right) e^{bt}, \tag{2}$$

  where ξ is the ratio of the longitudinal to transverse forward amplitudes, ϵ is the relative longitudinal polarisation of the virtual photon and M_ρ is the ρ^0 mass; the distribution of t, the square of the four-momentum transfer between the photon and the ρ^0, is described by a single exponential dependence, in the range from $t = 0$ to $t = -0.5$ GeV^2, with a slope parameter, $b \approx 7 - 12$ GeV^{-2};

- in real photoproduction ($Q^2 = 0$), the process is 'quasi-elastic' and the helicity of the ρ^0 is similar to that of the incident photon, i.e. s-channel helicity is largely conserved (SCHC) [8]. The ρ^0 decay distribution exhibits an approximate $\sin^2 \theta_h$ dependence, where θ_h is the polar angle of the π^+ in the ρ^0 c.m. system and the quantisation axis is the ρ^0 direction in the γp c.m. system;

- the real photoproduction ρ^0 total cross section increases slowly as a function of W for $W > 15$ GeV [9, 10]. This is expected for an elastic reaction dominated by the exchange of a 'soft' pomeron with an intercept of the Regge trajectory of $\alpha(0) = 1 + \epsilon' = 1.08$. The intercept is determined from fits [11] to hadron-hadron total cross sections: for a γp total cross section $\sigma_{tot} \sim W^{2(\alpha(0)-1)} \sim W^{2\epsilon'}$, the optical theorem yields $\left. \frac{d\sigma_{el}}{dt} \right|_{t=0} \sim W^{4\epsilon'} \sim W^{0.32}$.

At larger Q^2 ($2 < Q^2 < 25$ GeV^2), leptoproduction results from the EMC [6] and NMC [7] experiments indicate that:

- the $\gamma^* p \rightarrow \rho^0 p$ cross section is consistent with a $1/Q^4$ behaviour;

- at larger Q^2 (> 6 GeV^2), the distribution of the square of the transverse momentum of the ρ^0 with respect to the virtual photon (p_T^2) is exponentially falling with a slope of $b = 4.6 \pm 0.8$ GeV^{-2} [7], about a factor of two smaller than that of the photoproduction elastic process;

1

- as Q^2 increases, the fraction of zero-helicity, longitudinally polarised ρ^0s increases above 50%; assuming SCHC [1], this implies that the longitudinal virtual photon cross section dominates;

- for $2 < W < 4$ GeV the cross section falls with W at small $Q^2 < 4$ GeV^2 [4]. No significant dependence on W is observed for $9 < W < 19$ GeV [7].

The reaction $\gamma^* p \to \rho^0 p$ has also been the focus of theoretical investigations. Early studies based on VDM are described elsewhere [1]. A study of diffractive leptoproduction by Donnachie and Landshoff based on a zeroth order perturbative QCD (pQCD) calculation for pomeron exchange at small values of Bjorken $x \sim Q^2/W^2$ [11] reproduced many of the features seen experimentally, including the Q^2 dependence of the data at low W. In more recent presentations, the pomeron is treated as a non-perturbative two-gluon exchange [12]. This approach has also been studied by Cudell [13]. Calculations in pQCD have been performed in the leading logarithm approximation for J/ψ electroproduction by Ryskin [14]. Ginzburg et al. [15] and Nemchik et al. [16] have also performed a calculation in pQCD for vector meson production. These more recent calculations predict a Q^{-6} dependence of the longitudinal cross section at high Q^2, in contrast to the Q^{-4} VDM expectation. Brodsky et al. [17] have studied the forward scattering cross section for this reaction by applying pQCD in the double leading logarithm approximation (DLLA). They predict that at high Q^2 the vector mesons should be produced dominantly by longitudinally polarised virtual photons with a dependence for the longitudinal cross section:

$$\frac{d\sigma_L}{dt}\bigg|_{t=0} (\gamma^* N \to \rho^0 N) = \frac{A}{Q^6}\alpha_s^2(Q^2) \cdot \left|\left[1 + i(\pi/2)(\frac{d}{d\,ln\,x})\right] xg(x, Q^2)\right|^2, \tag{3}$$

where A is a constant, which can be calculated, and $xg(x, Q^2)$ is the momentum density of the gluon in the proton. Using the x-dependence of $xg(x, Q^2)$ measured at HERA and the relation $W^2 \sim Q^2/x$ for small x, at fixed Q^2 one expects that $\frac{d\sigma_{el}}{dt}\big|_{t=0} \sim W^{1.4}$ [18], in contrast to the $W^{0.32}$ dependence expected for the 'soft' pomeron.

This letter presents a measurement with the ZEUS detector of the exclusive cross section for ρ^0 mesons produced at large Q^2 by the virtual photoproduction process $\gamma^* p \to \rho^0 p$ at HERA. The data come from neutral current, deep inelastic electron-proton scattering in the Q^2 range of 7 - 25 GeV^2, similar to that of the earlier fixed target experiments [6, 7]; however, they cover a lower x region ($4 \cdot 10^{-4} < x < 1 \cdot 10^{-2}$) and, consequently, a higher W region (40-130 GeV).

2   Experimental conditions

The experiment was performed at the electron-proton collider HERA using the ZEUS detector. During 1993 HERA operated with bunches of electrons of energy $E_e = 26.7$ GeV colliding with bunches of protons of energy $E_p = 820$ GeV, with a time interval between bunch crossings of 96 ns. For this data-taking period 84 bunches were filled for each beam (paired bunches) and in addition 10 electron and 6 proton bunches were left unpaired for background studies. The electron and proton beam currents were typically 10 mA. The ep c.m. energy is $\sqrt{s} = 296$ GeV and the integrated luminosity was 0.55 pb^{-1}.

ZEUS is a multipurpose magnetic detector whose 1993 configuration has been described elsewhere [19]. This brief description concentrates on those parts of the detector relevant to the present analysis.

Charged particles are tracked by the inner tracking detectors which operate in a magnetic field of 1.43 T. Immediately surrounding the beampipe is the vertex detector (VXD) [20] which consists of 120 radial cells, each with 12 sense wires. Surrounding the VXD is the central tracking detector (CTD) [21] which consists of 72 cylindrical drift chamber layers, organised into 9 'superlayers'. In events with charged particle tracks, using the combined data from both chambers, resolutions of 0.4 cm in Z and 0.1 cm in radius in the XY plane[1] are obtained for the primary vertex reconstruction. These detectors provide a momentum resolution given by $\sigma_{p_T}/p_T = \sqrt{(0.005 p_T)^2 + (0.016)^2}$ (with p_T in GeV).

The superconducting solenoid is surrounded by a high resolution uranium/scintillator calorimeter which is divided into three parts: forward (FCAL), barrel (BCAL), and rear (RCAL) covering the angular region $2.2^\circ < \theta < 176.5^\circ$, where $\theta = 0^\circ$ is defined as the proton beam direction. Holes of 20×20 cm^2 in the centre of FCAL and RCAL are required to accommodate the HERA beam pipe. The calorimeter parts are subdivided into towers which in turn are subdivided longitudinally into electromagnetic (EMC) and hadronic (HAC) sections. The sections are subdivided into cells, each of which is viewed by two photomultiplier tubes which provide the energy and the time of the energy deposit with a resolution of better than 1 ns. An additional hadron-electron separator (RHES)[22], located at the electromagnetic shower maximum in the RCAL and consisting of a layer of 3×3 cm^2 silicon diodes, was used to provide more accurate position information for electrons scattered at low angles than was available from the calorimeter alone.

The luminosity is measured from the rate observed in the luminosity photon detector of hard bremsstrahlung photons from the Bethe-Heitler process $ep \to ep\gamma$. The luminosity detector consists of photon and electron lead-scintillator calorimeters [23]. Bremsstrahlung photons emerging from the electron-proton interaction point at angles below 0.5 mrad with respect to the electron beam axis hit the photon calorimeter placed 107 m along the electron beam line. Electrons emitted at scattering angles less than 5 mrad and with energies $0.2 E_e < E'_e < 0.9 E_e$ are deflected by beam magnets and hit the electron calorimeter placed 35 m from the interaction point.

The data were collected with a three-level-trigger. The first-level-trigger (FLT) for DIS events required a logical OR of three conditions on sums of energy in the EMC calorimeter cells. Details are given elsewhere [19, 24]. For events with the scattered electron detected in the calorimeter, the FLT was essentially independent of the DIS hadronic final state. The FLT acceptance was greater than 97% for $Q^2 > 7$ GeV^2. The second-level-trigger used information from a subset of detector components to reject proton beam-gas events, thereby reducing the FLT DIS triggers by an order of magnitude, but without loss of DIS events.

The third-level-trigger (TLT) had available the full event information on which to apply physics-based filters. The TLT applied stricter cuts on the event times and also rejected beam-halo muons and cosmic ray muons. Events remaining after the above veto cuts were selected for output by the TLT if $\delta \equiv \Sigma_i E_i (1 - \cos\theta_i) > 20$ GeV $- 2E_\gamma$, where E_i, θ_i are the energy and polar angle (with respect to the nominal beam interaction point) of the geometric centre of a calorimeter cell and E_γ is the energy measured in the photon calorimeter of the luminosity monitor. For fully contained events $\delta \sim 2E_e = 53.4$ GeV. For events from photoproduction, the scattered electrons remain in the rear beam pipe and δ peaks at low values.

---

[1]The ZEUS coordinate system is defined as right-handed with the Z axis pointing in the proton beam direction, hereafter referred to as forward, and the X axis horizontal, pointing towards the centre of HERA.

3 Kinematics of exclusive ρ^0 production

The kinematic variables used to describe ρ^0 production in the reaction:

$$e \; + \; p \rightarrow e \; + \; \rho^0 \; + X, \tag{4}$$

where X represents either a proton or a diffractively dissociated proton remnant of mass M_X, are the following: the negative of the squared four-momentum transfer carried by the virtual photon[2] $Q^2 = -q^2 = -(k - k')^2$, where k (k') is the four-momentum of the incident (scattered) electron; the Bjorken variable $x = \frac{Q^2}{2P \cdot q}$, where P is the four-momentum of the incident proton; the variable which describes the energy transfer to the hadronic final state $y = \frac{q \cdot P}{k \cdot P}$; the c.m. energy, $\sqrt{s}$, of the ep system, where $s = (k + P)^2$; W, the c.m. energy of the $\gamma^* p$ system: $W^2 = (q + P)^2 = \frac{Q^2(1-x)}{x} + M_p^2 \approx ys$, where M_p is the proton mass; and $t' = |t - t_{min}|$, where t is the four-momentum transfer squared, $t = (q - v)^2 = (P - P')^2$, from the photon to the ρ^0 (with four-momentum v), t_{min} is the minimum kinematically allowed value of t and P' is the four-momentum of the outgoing proton. The squared transverse momentum p_T^2 of the ρ^0 with respect to the photon direction is a good approximation to t' since t' is, in general, small ($<< 1$ GeV^2). For the present data[3] t_{min} ranges from -0.0006 to -0.08 GeV^2.

In this analysis, the ρ^0 was observed in the decay $\rho^0 \rightarrow \pi^+\pi^-$. The momentum vector of the ρ^0 was reconstructed from the pion momentum vectors determined with the tracking system. The production angles (θ_ρ and ϕ_ρ) and momentum (p_ρ) of the ρ^0 and the angles of the scattered electron (θ_e' and ϕ_e'), as determined with RCAL and RHES, were used to reconstruct the kinematic variables x, Q^2, etc. The energy of the scattered electron was determined from the relation:

$$E_e^c = \frac{(s + M_{\pi\pi}^2 - M_X^2)/2 - (E_e + E_p)(E_\rho - |p_\rho|cos\theta_\rho)}{(E_e + E_p)(1 - \beta cos\theta_e') - (E_\rho - |p_\rho|cos\theta_{e\rho})}, \tag{5}$$

where E_ρ is the energy of the $\pi\pi$ pair, $\theta_{e\rho}$ is the angle between the $\pi\pi$ three vector and the scattered electron and $\beta = (E_p - E_e)/(E_p + E_e)$. For the case of reaction (1), $M_X = M_p$ and E_e^c is a good estimator of the energy of the scattered electron, E_e'; for events in which the proton diffractively dissociates into the system X, $M_X > M_p$ and E_e^c is only slightly different from E_e'. The above expression simplifies to

$$E_e^c \approx [2E_e - (E_\rho - |p_\rho|cos\theta_\rho)]/(1 - cos\theta_e') \tag{6}$$

when $M_X = M_p$ and the transverse momentum of the proton is negligible compared to its longitudinal component. This last relation provides an accurate way to calculate the kinematic variables and is a simple expression used to evaluate the radiative corrections for this process. The variable y is calculated from the expression $y = (E_\rho - |p_\rho|cos\theta_\rho)/2E_e$. The calculation of p_T^2 also uses the ρ^0 and electron momenta: $p_T^2 = (p_{ex} + p_{\rho x})^2 + (p_{ey} + p_{\rho y})^2$.

4 Monte Carlo simulations

The reaction $ep \rightarrow e\rho^0 p$ was modelled using two different Monte Carlo generators. The first, DIPSI [25], describes elastic ρ^0 production in terms of pomeron exchange with the pomeron treated as a colourless two-gluon system [14]. The model assumes that the exchanged photon

---

[2]In the Q^2 range covered by this data sample, effects due to Z^0 exchange can be neglected.

[3]The -0.08 GeV^2 value corresponds to $M_X = 8$ GeV and $Q^2 = 25$ GeV^2.

fluctuates into a quark-antiquark pair which then interacts with the two-gluon system. The cross section is proportional to the square of the gluon momentum density in the proton. Samples of ϕ and ω events were generated in a similar way.

A second sample of ρ^0 events was generated with a Q^{-6} dependence for the ep reaction, a flat helicity angular distribution, and an exponentially falling p_T^2 distribution with a slope of $b = 5$ GeV^{-2}. The Monte Carlo generator used the HERWIG framework [26] and the events were weighted according to the measured helicity, p_T^2 and y distributions.

A third ρ^0 Monte Carlo generator (RHODI), based on the model of Forshaw and Ryskin [27], was used to model the proton dissociative processes with a $d\sigma(\gamma^*p)/dM_X^2 \propto 1/M_X^{2.5}$ dependence. Different M_X dependences were obtained by weighting the events. Events were generated for M_X^2 values between 1.2 and 4000 GeV^2. All Monte Carlo events were passed through the standard ZEUS detector and trigger simulation programs and through the event reconstruction software.

The radiative corrections were calculated to be (10-15)% for the selection cuts used in the analysis and for the Q^2 and W dependences found in the data. They are taken into account in the cross sections given below.

5   Analysis and cross sections

5.1   Data selection

For the selection of exclusive ρ^0 candidates, the off-line analysis required:

- a scattered electron energy, as measured in the calorimeter, greater than 5 GeV. The electron identification algorithms used in this analysis were optimised to have high efficiency ($> 97\%$);

- $\delta = \sum_i E_i(1 - \cos\theta_i) > 35$ GeV, where the sum runs over all calorimeter cells; this cut reduces the radiative corrections and photoproduction background;

- two tracks with opposite charge, both associated with the reconstructed vertex; if there was a third track at the vertex, it should be from the scattered electron. Each of the two tracks was required to have a transverse momentum above 0.16 GeV and a polar angle between 25º and 155º; this corresponds to the region where the CTD response and systematics are well understood;

- a measured vertex (Z_{vtx}), as reconstructed from VXD and CTD tracks, to be in the range $-50 < Z_{vtx} < 40$ cm;

- events with a scattered electron whose impact point in the RCAL was outside the square of 32×32 cm^2 centered on the beam axis or events with an RHES impact point outside the square of 26×26 cm^2; this requirement controls the determination of the electron scattering angle; and

- the residual calorimeter energy not associated with the electron to be compatible with the ρ^0 momentum measured in the tracking system, $E_{CAL}^\rho/P_\rho < 1.5$ (see Fig. 1a), where E_{CAL}^ρ is the calorimeter energy excluding that due to the scattered electron and P_ρ is the sum of the absolute values of the momenta of the two oppositely charged tracks. This cut suppresses backgrounds with additional calorimeter energy unmatched to the tracks

and events with proton dissociation depositing energy in the calorimeter towers around the FCAL beampipe. Also shown in Fig. 1a is the distribution from the ρ^0 DIPSI Monte Carlo events, indicating that only a small fraction of the exclusive ρ^0 events are removed by this cut. Fig. 1b shows the same distribution after the final selection indicating good agreement with the expected distribution.

A total of 352 events passed these selection requirements.

Possible backgrounds to the exclusive reaction (1) are from ρ^0 events with additional undetected particles, from ϕ and ω production and from proton dissociation events where M_X is small and therefore does not deposit energy in the calorimeter. To reduce these backgrounds, two additional cuts were imposed:

- $0.6 < M_{\pi^+\pi^-} < 1.0$ GeV; this selection reduces the contamination from ϕ and ω production in the low $\pi^+\pi^-$ mass region as well as higher mass resonant states and non-exclusive events in the high mass region; and

- $p_T^2 < 0.6$ GeV^2; this cut reduces non-exclusive background and proton dissociation events. Fig. 1c shows the measured, uncorrected p_T^2 distribution for the selected ρ^0 events, indicating a clear excess of events above a single exponential for $p_T^2 > 0.6$ GeV^2, consistent with the presence of proton dissociation events which, in hadron-hadron scattering, have a less steep p_T^2 distribution [28]. (The acceptance is relatively flat, rising by about 5% from $p_T^2 = 0$ to 0.6 GeV^2.)

Fig. 1d shows a scatter plot of Q^2 versus x for the 140 events which pass the above criteria. The efficiency drops sharply at small Q^2 (due to the cut on the electron impact point in RCAL) and at small and large y (due to the requirements on the π^+, π^- tracks). To remove poorly reconstructed events and to select a region of phase space where the acceptance is well determined and relatively constant as a function of the kinematic variables, two additional kinematic cuts were applied to the data:

- $7 < Q^2 < 25$ GeV^2 and $0.02 < y < 0.20$.

The final ρ^0 sample contains 82 events.

5.2 Background estimates and acceptance corrections

The DIPSI ρ^0 Monte Carlo simulated events were used to correct the data for acceptance and detector resolution. The acceptance (which includes the geometric acceptance, reconstruction efficiencies, detector efficiency and resolution, corrections for the offline analysis cuts and a correction for the $M_{\pi^+\pi^-}$ cut) in this region of Q^2 varies between 40% and 55%. The acceptance is constant at about 47% as a function of y, p_T^2 or $M_{\pi^+\pi^-}$ in the above kinematic region. The resolutions in the measured kinematic variables, as determined from the Monte Carlo events, are 6% for Q^2 and 2% for y.

Fig. 2a, which shows the uncorrected $\pi^+\pi^-$ mass distribution for the events passing all of the final cuts (except for the $M_{\pi^+\pi^-}$ cut, but with a $M_{K^+K^-} > 1.05$ GeV cut, when the tracks are assigned a kaon mass, to remove ϕ events), indicates a pure sample of ρ^0 events. A ρ^0 non-relativistic Breit-Wigner form, with a constant background, is fit to the mass spectrum between 0.6 and 2.0 GeV. The resulting parameters for the ρ^0 mass and width are 774 ± 9 MeV and 134 ± 20 MeV, respectively, to be compared with the values 769.9 MeV and 151.2 MeV from the Particle Data Group [29]. The fit also includes a flat background estimate of $(4 \pm 4)\%$

6

for $M_{\pi^+\pi^-}$ masses between 0.6 and 1.0 GeV, as determined from comparing the Monte Carlo ρ^0 events with the data for $M_{\pi^+\pi^-}$ masses between 1.0 and 1.5 GeV. Background contributions from exclusive ϕ and ω events were estimated to be at the 1% level and are included in the above background estimate.

Since the proton was not detected, the proton dissociation background contribution had to be subtracted. This was done using the RHODI event generator combined with the detector simulation. The normalisation was obtained by requiring that the Monte Carlo generated sample have the same number of events with energy between 1 and 20 GeV in the FCAL as for the data (7 events) when the constraint that $E^\rho_{CAL}/P_\rho < 1.5$ was relaxed to $(E^\rho_{CAL} - E_{FCAL})/P_\rho < 1.5$ and the additional constraint $\theta_{\pi\pm} > 50^o$ was imposed. Assuming an M_X dependence of the form $1/M_X^{2.25}$, as measured by the CDF experiment [30] for $\overline{p}p \rightarrow \overline{p} + \text{X}$, yielded a contribution of $(22 \pm 8 \pm 15)\%$ where the systematic error was obtained from varying the exponent of $1/M_X$ between 2 and 3. This is consistent with an estimate from the excess above the exponential in the p_T^2 distribution mentioned above. In the exclusive ρ^0 sample under study here, there are no events with an electron energy in the range $5 < E'_e < 14$ GeV and so the photoproduction background is negligible. No events were found from the unpaired bunches demonstrating that the beam-gas background is also negligible. The overall background contamination was estimated to be $\Delta = (26 \pm 18)\%$. Unless explicitly stated otherwise, this background was subtracted as a constant fraction for the cross sections given below.

5.3   The ep cross section

The cross section, measured in the kinematic region defined above, is obtained from $\sigma(ep \rightarrow e\rho^0 p) = N(1 - \Delta)C_1/(C_2 \cdot A \cdot L_{int})$, where N ($= 82$) is the observed number of events after all cuts with $0.6 < M_{\pi\pi} < 1.0$ GeV, Δ is the background estimation, A is the acceptance as discussed above, L_{int} is the integrated luminosity of 0.55 pb^{-1} and C_2 is the correction for QED radiative effects. These radiative corrections were calculated for the exclusive reaction using the x and Q^2 dependences found in this experiment (see section 6.1) and vary between 1.10 (at low Q^2 and low y) and 1.14 (at high Q^2 and high y). A systematic uncertainty of ± 0.10 was included on this correction to account for the uncertainties in the cross section dependences on x and Q^2. To compare later with results from the NMC experiment, which has determined exclusive ρ^0 cross sections integrated over all p_T^2 [7], C_1 is a 4.5% correction for the cross section in the p_T^2 range between 0.6 and 1.0 GeV^2 based on the slope of the distribution measured in the present analysis. The corrected ep cross section for exclusive ρ^0 production at $\sqrt{s} = 296$ GeV is

$$\sigma(ep \rightarrow e\rho^0 p) = 0.21 \pm 0.03(stat.) \pm 0.06(syst.) \text{ nb},$$

integrated over the ranges $7 < Q^2 < 25$ GeV^2, $0.02 < y < 0.20$ and $p_T^2 < 1.0$ GeV^2, with acceptance corrected $< Q^2 >$ and $< W >$ of 11.0 GeV^2 and 78.9 GeV, respectively.

The quoted systematic uncertainty is derived from the following (the systematic uncertainty for each item is indicated in parentheses):

- the cuts used to remove non-exclusive backgrounds were varied and independent analyses using differing selection cuts and background estimates were compared to the previously described analysis: tracks were matched to the calorimeter energy deposits and events containing an energy in excess of that of the ρ^0 of more than 0.4, 1 or 2 GeV were discarded; events were selected based on the position of the electron measured by the calorimeter rather than by the RHES and the cut on the impact position of the electron in RCAL was varied (10%);

7

- using different trigger configurations (8%),

- the cuts on the tracks were varied. The lower cut on the transverse momentum was varied between 0.1 and 0.2 GeV and different polar angle selections were made. The maximum variation occurred for $p_T > 0.2$ GeV (9%); and

- events from different Monte Carlo generators were used to calculate the acceptance and efficiency (7%).

Adding these in quadrature to those from the uncertainties due to background subtraction (24%), luminosity (3.3%) and radiative corrections (10%) yields 31% as the overall systematic uncertainty.

5.4 The $\gamma^* p$ cross sections

The ep cross section was converted to a $\gamma^* p$ cross section as follows. The differential ep cross section for one photon exchange can be expressed in terms of the transverse and longitudinal virtual photoproduction cross sections (see [2]) as:

$$\frac{d^2\sigma(ep)}{dx dQ^2} = \frac{\alpha}{2\pi x Q^2} \left[\left(1 + (1-y)^2\right) \cdot \sigma_T^{\gamma^* p}(y, Q^2) + 2(1-y) \cdot \sigma_L^{\gamma^* p}(y, Q^2) \right].$$

The virtual photon-proton cross section can then be written in terms of the electron-proton differential cross section:

$$\sigma(\gamma^* p \to \rho^0 p) = (\sigma_T^{\gamma^* p} + \epsilon \sigma_L^{\gamma^* p}) = \frac{1}{\Gamma_T} \frac{d^2\sigma(ep \to e\rho^o p)}{dx dQ^2} \tag{7}$$

where Γ_T, the flux of transverse virtual photons, and ϵ, the ratio of the longitudinal to transverse virtual photon flux, are given by

$$\Gamma_T = \frac{\alpha \left(1 + (1-y)^2\right)}{2\pi x Q^2} \quad \text{and} \quad \epsilon = \frac{2(1-y)}{(1 + (1-y)^2)}.$$

Throughout the kinematic range studied here, ϵ is in the range $0.97 < \epsilon < 1.0$.

Using Eq. (7), $\sigma(\gamma^* p \to \rho^0 p)$ was determined with the flux calculated from the Q^2, x and y values on an event-by-event basis. The 31% overall systematic uncertainty on $\sigma(ep)$ applies to every value for $\sigma(\gamma^* p \to \rho^0 p)$ and thus becomes an overall normalisation uncertainty.

6 Results

6.1 Q^2 and p_T^2 distributions

After correcting for detector acceptance and backgrounds, the cross sections were obtained as a function of Q^2. Fig. 2b displays the Q^2 dependence of the $\gamma^* p \to \rho^o p$ cross section for events in the x range between 0.0014 and 0.004. Also displayed in Fig. 2b are data from the NMC experiment [7]. The ZEUS values of the cross sections are larger than those of the NMC experiment. However, it should be noted that for this figure as well as for Figs. 2d, 3 and 4 the different experiments have different mixtures of longitudinal and transverse photon fluxes (ϵ varies from 0.5-0.8 for the NMC results). More importantly, the region of $\gamma^* p$ c.m. energy of the NMC experiment (8-19 GeV) is lower than that in this experiment (40-130 GeV).

A fit of the form $Q^{-2\alpha}$ to the distribution of the ZEUS data in Fig. 2b yields the power of the Q^2 dependence. To study the systematic uncertainty on the value of α, a maximum likelihood analysis was performed with the cross section factorised as:

$$\sigma(\gamma^*p \to \rho^0 p) \sim (Q^2)^{-\alpha} \cdot x^{-\beta} \cdot e^{-bp_T^2}. \tag{8}$$

This study, applied to the 82 events in the final data sample in the region $0.02 < y < 0.20$, $p_T^2 < 0.6$ GeV^2 and $7 < Q^2 < 25$ GeV^2, yields results similar to those obtained from fitting Fig. 2b. The best estimate of the Q^2 dependence is $2\alpha = 4.2 \pm 0.8(stat.)^{+1.4}_{-0.5}(syst.)$, where the systematic uncertainty comes from the variation in the value of α obtained from the two different fitting methods as well as from the variation obtained from the systematic studies described in section 5.3.

The uncorrected p_T^2 distribution was presented in Fig. 1c and showed an exponentially falling behaviour, with an excess of events for $p_T^2 > 0.6$ GeV^2, as discussed previously. After correcting for detector acceptance and resolution, a fit in the range $0 < p_T^2 < 1.0$ GeV^2 of the form:

$$\frac{d\sigma}{dp_T^2} = Ae^{(-bp_T^2)} + Be^{(-\frac{b}{2}p_T^2)}, \tag{9}$$

was performed. In Eq. (9) the contribution from the second term, which was constrained to be 22% of the number of events for $p_T^2 < 0.6$ GeV^2, represents the proton dissociative background contribution which was assumed to have a slope half that of the exclusive reaction [28]. The fit yields a slope parameter of $b = 5.1^{+1.2}_{-0.9}(stat.) \pm 1.0(syst.)$ GeV^{-2}, which is consistent with that found in the maximum likelihood fit. The systematic uncertainty comes from the variation in the value of b obtained from fits without the second term in Eq. (9), the maximum likelihood fit and from the systematic studies described in section 5.3. This value of b is about half that found in elastic ρ^0 photoproduction [10] and is in agreement with the result from the NMC experiment [7].

6.2 ρ^0 decay distribution

The ρ^0 s-channel helicity decay angular distribution $H(\cos\theta_h, \phi_h, \Phi_h)$ can be used to determine the ρ^0 spin state [31], where θ_h and ϕ_h are the polar and azimuthal angles, respectively, of the π^+ in the ρ^0 c.m. system and Φ_h is the azimuthal angle of the ρ^0 production plane with respect to the electron scattering plane. The quantisation axis is defined as the ρ^0 direction in the γ^*p c.m. system. Only the $\cos\theta_h$ dependence is presented here. After integrating over ϕ_h and Φ_h, the decay angular distribution can be written as:

$$\frac{1}{N}\frac{dN}{d\cos\theta_h} = \frac{3}{4}[1 - r_{00}^{04} + (3r_{00}^{04} - 1)\cos^2\theta_h], \tag{10}$$

where the density matrix element r_{00}^{04} represents the probability that the ρ^0 was produced longitudinally polarised by either transversely or longitudinally polarised virtual photons.

The helicity $\cos\theta_h$ distribution (uncorrected for background, since the dominant contribution to the background is from proton dissociation which is expected to have the same helicity as the $\rho^0 p$ final state) is shown in Fig. 2c. The curve shown in the figure is from a maximum likelihood fit to the form of Eq. (10) yielding $r_{00}^{04} = 0.6 \pm 0.1^{+0.2}_{-0.1}$ at $< Q^2 > = 11.0$ GeV^2 and $< W > = 78.9$ GeV, where the first uncertainty is statistical, and the second is derived from the variations of the result when different ranges in $\cos\theta_h$ were used in the fit and when the

9

systematic studies of section 5.3 were used. In Fig. 2d this measurement of r_{00}^{04} is compared to other published data at various values of Q^2. These data show the presence of both transversely and longitudinally polarised ρ^0's at high Q^2 (above 2 GeV^2). If SCHC is assumed, an estimate of R, the ratio of longitudinal to transverse cross sections, for ρ^0 production is obtained [2]:

$$R = \frac{\sigma_L}{\sigma_T} = \frac{1}{\epsilon} \cdot \frac{r_{00}^{04}}{1 - r_{00}^{04}} = 1.5^{+2.8}_{-0.6}$$

(where the statistical and systematic uncertainties in r_{00}^{04} have been added in quadrature). This may be compared with the value of $R = 2.0 \pm 0.3$ at $< Q^2 > = 6$ GeV^2 and $< W > \sim 14$ GeV from the NMC experiment [7].

6.3 The W and x dependences of the $\gamma^* p \to \rho^0 p$ cross section

Fig. 3 shows a compilation [2,4,5,7-9] of photoproduction and selected leptoproduction exclusive ρ^0 cross sections as a function of both Q^2 and W. In this figure the cross sections obtained in this analysis are shown as a function of W at $Q^2 = 8.8$ and 16.9 GeV^2. The cross sections at different W values (and slightly different $< Q^2 >$) were scaled to $Q^2 = 8.8$ and 16.9 GeV^2 using the measured $Q^{-4.2}$ dependence in order to compare with the NMC cross sections[4] from deuterium at the same values of Q^2. At high energies, $W > 50$ GeV, data exist only at $Q^2 = 0$, 8.8 and 16.9 GeV^2. The real ($Q^2 = 0$) γp 'elastic' cross section [10] shows only a slow rise, consistent with that seen in the photon-proton total cross section. At small Q^2 (< 2.6 GeV^2), the data first decrease with increasing W followed by a slow increase. No high energy data are yet available to see how the increase develops. At higher Q^2, the cross sections rise strongly with increasing W. At $Q^2 = 8.8$ GeV^2 and $W \sim 100$ GeV, the cross section is about a factor of six larger than at $W = 12.9$ GeV [7]. This strong increase in the $\gamma^* p \to \rho^0 p$ cross section is in contrast to that expected from the Donnachie and Landshoff model [11, 12].

To compare with the QCD calculations of Brodsky et al. and Donnachie and Landshoff, the ZEUS and NMC cross sections are shown as a function of x at $Q^2 = 8.8$ and 16.9 GeV^2 in Figs. 4a, b. The total cross sections are predicted from the pQCD calculations of Brodsky et al. [17] using the longitudinal contribution to the differential cross section at $t = 0$, (see Eq. (3)):

$$\sigma(x, Q^2) = \int_0^1 \frac{d\sigma(x, Q^2, p_T^2)}{dp_T^2} dp_T^2 = \frac{(1 - e^{-b})}{b} \cdot \left. \frac{d(\sigma_T + \sigma_L)}{dt} \right|_{t=0} = \frac{(1 - e^{-b})}{b} \cdot \left(\frac{1}{R} + \epsilon \right) \cdot \left. \frac{d\sigma_L}{dt} \right|_{t=0}$$
(11)

where b is the slope of the p_T^2 distribution. The measured values of $\epsilon = 0.98$, $R = 1.5$ and $b = 5.1$ GeV^{-2} were used to calculate $\sigma(x, Q^2)$. For the gluon momentum density, $xg(x, Q^2)$, the form $xg \sim x^\delta \cdot (1 - x)^\eta$ was assumed. The values of δ and η were allowed to vary within the ranges (-0.25 to -0.39) and (6.44 to 4.81) respectively. These ranges were determined from the leading order gluon density extracted [18] from the scaling violations of the ZEUS F_2 measurements [19]. The uncertainty in Eq. (11) arising from the 1σ range in the gluon density[18] is shown as the light shaded region in Fig. 4. The uncertainty in the prediction arising from measurement uncertainties of R and b when added in quadrature to that of the gluon distribution yields the larger dark shaded area. The shaded areas in Fig. 4 are restricted to $x < 0.01$ where Eq. (3) is valid. The range in the predicted cross sections at a given x is dominated by the uncertainty on δ. Since the calculation is made in DLLA, the value of

---

[4]Since the EMC and NMC data cover approximately the same kinematic region, the more recent NMC data[7] have been chosen to make comparisons.

Q^2 at which the gluon density and α_s are evaluated is not defined to better than a factor of two. Varying the Q^2 scale for $\alpha_s(Q^2) \cdot xg(x, Q^2)$ from $Q^2/2$ to $2Q^2$ changes the prediction by about 50%. The x scale in the calculation can also range from $x/2$ to $2x$ so that the curves can be shifted left or right to reflect this uncertainty. At the present level of precision of the measurement and theory, the data are consistent with the pQCD calculation of Brodsky et al. The hatched region shows the range of the predictions of Donnachie and Landshoff based on soft pomeron exchange [11] with $\sigma = \frac{1}{b} \left. \frac{d\sigma}{dt} \right|_{t=0}$. The range of the hatched area comes from the uncertainty in the measured value of b. The data do not agree with these expectations, being typically a factor of three above the predictions.

7   Conclusions

Exclusive ρ^0 production has been studied in deep inelastic electron-proton scattering at large Q^2 (7 - 25 GeV^2) in the $\gamma^* p$ centre of mass energy (W) range from 40 to 130 GeV. Cross sections are given for both the ep and $\gamma^* p$ processes. The cross section for the $\gamma^* p$ process exhibits a $Q^{-(4.2 \pm 0.8^{+1.4}_{-0.5})}$ dependence. The $\gamma^* p \to \rho^0 p$ cross section at these large Q^2 values shows a strong increase with W at HERA energies over the lower energy NMC data, in contrast to the behaviour of the elastic photoproduction cross section. Both longitudinally and transversely polarised ρ^0's are produced. The Q^2 dependence, the polarisation and the slope of the p_T^2 distribution are consistent with those observed at lower energies. However, the cross sections are significantly larger. The Donnachie and Landshoff prediction for soft pomeron exchange underestimates the measured cross sections while the data are consistent with the perturbative QCD calculation of Brodsky et al. given the present knowledge of the gluon momentum density in the proton.

Acknowledgements

References

[1] T. H. Bauer et al., Rev. Mod. Phys. 50 (1978) 261.

[2] P. Joos et al., Nucl. Phys. B113 (1976) 53.

[3] C. del Papa et al., Phys. Rev. D19 (1979) 1303.

[4] D. G. Cassel et al., Phys. Rev. D24 (1981) 2787.

[5] W. D. Shambroom et al., Phys. Rev. D26 (1982) 1.

[6] EMC Collab., J. J. Aubert et al., Phys. Lett. 161B (1985) 203;
J. Ashman et al., Z. Phys. C39 (1988) 169.

[7] NMC Collab., P. Amaudruz et al., Z. Phys. C54 (1992) 239;
M. Arneodo et al., Nucl. Phys. B429 (1994) 503.

[8] J. Ballam et al., Phys. Rev. Lett. 24 (1970) 960.

[9] "Total Cross-Sections for Reactions of High Energy Particles", Landolt-Börnstein, New Series, Vol. 12b, editor H. Schopper (1987).

[10] ZEUS Collab., M. Derrick et al., "Measurement of the elastic ρ^0 photoproduction cross section at HERA", paper ICHEP94 Ref. 0688, submitted to the 27th International Conference on High Energy Physics, Glasgow (1994);
ZEUS Collab., M. Derrick et al., Z. Phys. C63 (1994) 391.

[11] A. Donnachie and P. V. Landshoff, Phys. Lett. B185 (1987) 403.

[12] A. Donnachie and P. V. Landshoff, Nucl. Phys. B311 (1989) 509; Phys. Lett. B348 (1995) 213.

[13] J. R. Cudell, Nucl. Phys. B336 (1990) 1.

[14] M. G. Ryskin, Z. Phys. C57 (1993) 89; and private communication.

[15] I. F. Ginzburg et al., "Semihard quasidiffractive production of neutral mesons by off shell photons", preprint, submitted to Nucl. Phys. B (1994).

[16] J. Nemchik et al., Phys. Lett. B341 (1994) 228.

[17] S. J. Brodsky et al., Phys. Rev. D50 (1994) 3134.

[18] ZEUS Collab., M. Derrick et al., Phys. Lett. B345 (1995) 576.

[19] ZEUS Collab., M. Derrick et al., Z. Phys. C65 (1995) 379.

[20] C. Alvisi et al., Nucl. Instr. and Meth. A305 (1991) 30.

[21] C. B. Brooks et al., Nucl. Instr. and Meth. A283 (1989) 477;
B. Foster et al., Nucl. Instr. and Meth. A338 (1994) 254.

[22] ZEUS Collab., The ZEUS Detector Status Report 1993.

[23] J. Andruszków et al., DESY 92–066 (1992).

[24] W. H. Smith et al., Nucl. Instr. and Meth. A355 (1995) 278.

[25] M. Arneodo, L. Lamberti and M. G. Ryskin, to be submitted to Comp. Phys. Comm. (1995).

[26] G. Marchesini et al., Comp. Phys. Comm. 67 (1992) 465.

[27] J. R. Forshaw and M. G. Ryskin, DESY 94-162 and private communication.

[28] K. Goulianos, Phys. Rep. 101 (1983) 169.

[29] Review of Particle Properties, Particle Data Group, Phys. Rev. D50 (1994) 1664.

[30] CDF Collab., F. Abe et al., Phys. Rev. D50 (1994) 5535.

[31] K. Schilling, P. Seyboth and G. Wolf, Nucl. Phys. B15 (1970) 397;
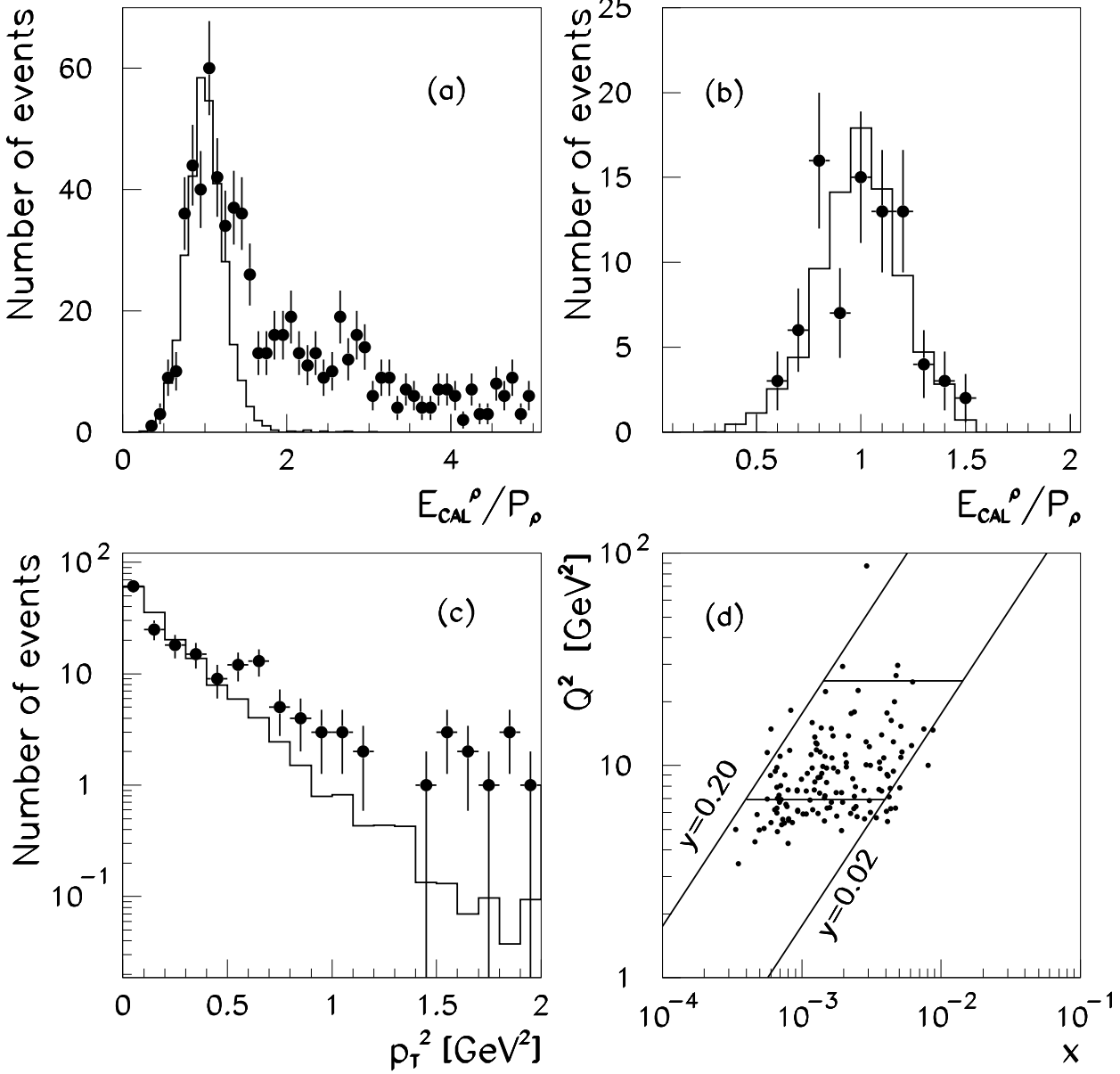K. Schilling and G. Wolf, Nucl. Phys. B61 (1973) 381.

Figure 1: (a) The distribution of E_{CAL}^{ρ}/P_{ρ} for the candidate events; (b) the same distribution for the final sample of 82 events; (c) the p_T^2 distribution; and (d) a scatter plot of Q^2 versus x for the selected ρ^0 events. These plots are not corrected for detector and trigger efficiencies and acceptances. The histograms in (a-c) are obtained from the DIPSI ρ^0 Monte Carlo sample after detector and trigger simulation. In (d) the lines correspond to the region in Q^2 and y selected for this analysis.
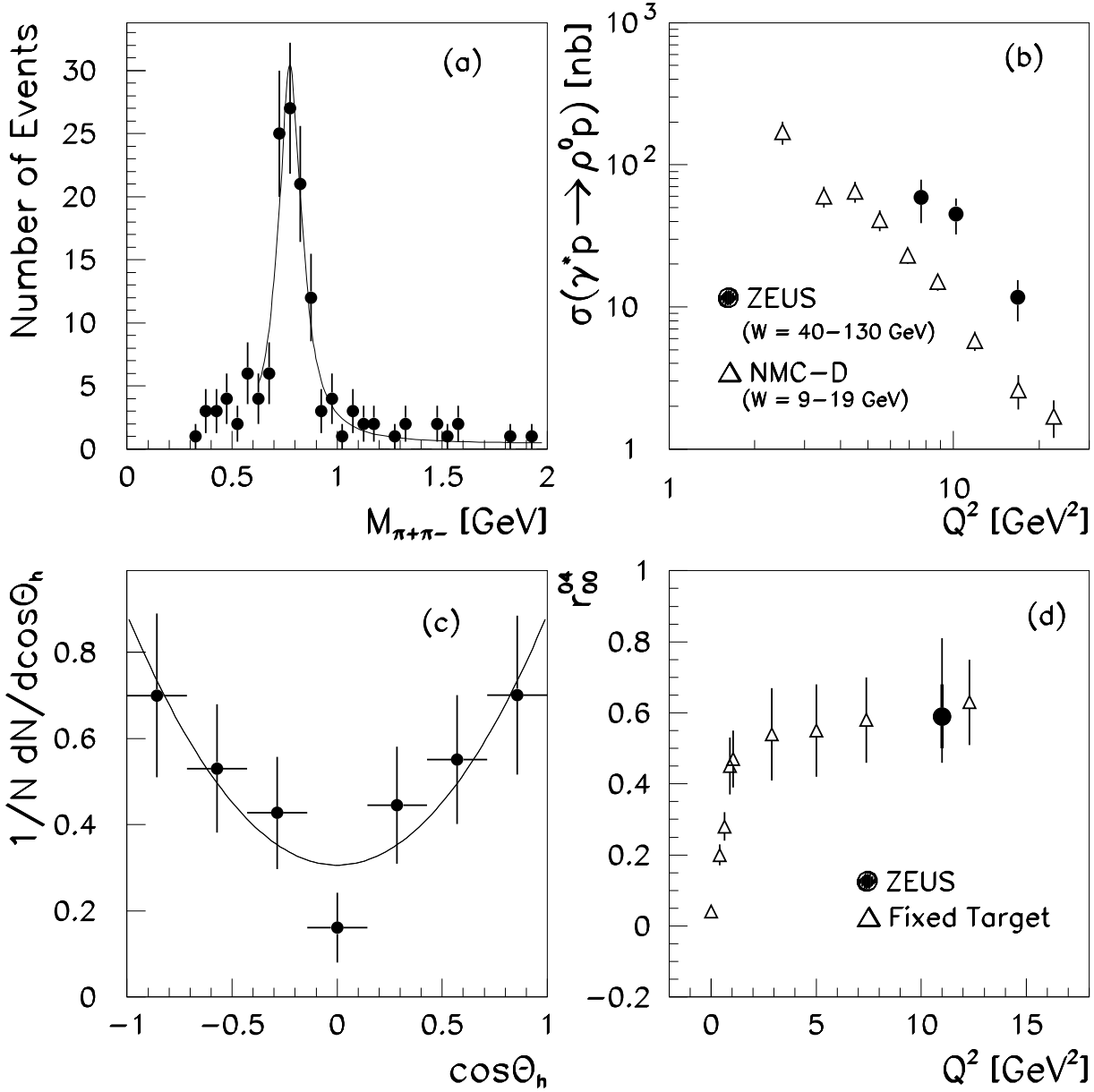
14

Figure 2: (a) The $\pi^+\pi^-$ invariant mass distribution for the final sample of events; the curve is a maximum likelihood fit with a non-relativistic Breit-Wigner distribution plus a flat (4%) background (see text for details); (b) the cross section for $\gamma^*p \to \rho^0 p$ as a function of Q^2 for $0.0014 < x < 0.004$. Also shown are data from the NMC experiment [7]; the errors shown are just the statistical errors. The ZEUS (NMC) data have an additional 31% (20%) normalisation uncertainty (not shown); (c) the $\cos\theta_h$ distribution for the decay π^+, in the s-channel helicity system, corrected for acceptance, for $\pi^+\pi^-$ pairs in the mass range 0.6-1.0 GeV. The curve is a fit to the form of Eq. (10); (d) the ρ^0 density matrix element, r^{04}_{00}, compared with results from fixed target experiments [2,3,7] as a function of Q^2. The thick error is the statistical error and the thin error is the systematic error added in quadrature.
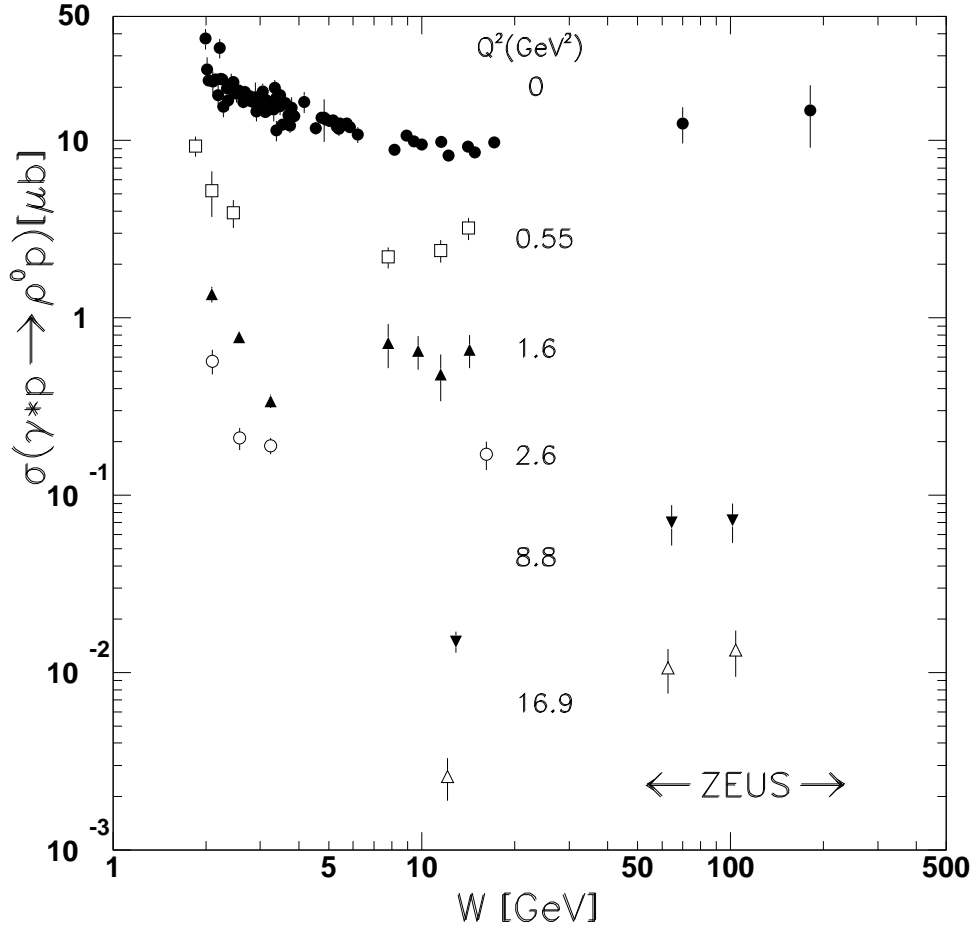
Figure 3: The $\gamma^*p \to \rho^0 p$ cross section as a function of W, the γ^*p centre of mass energy, for several values of Q^2. The low energy data ($W < 20$ GeV) come from fixed target experiments [2,4,5,7,8]. The high energy data ($W > 50$ GeV) come from the ZEUS experiment [10] and the present analysis. The ZEUS data at $Q^2 = 8.8$ and 16.9 GeV^2 have an additional 31% systematic normalisation uncertainty (not shown); the data from Refs. [2], [4] and [7] have additional 10%, 25%, and 20% normalisation uncertainties, respectively.
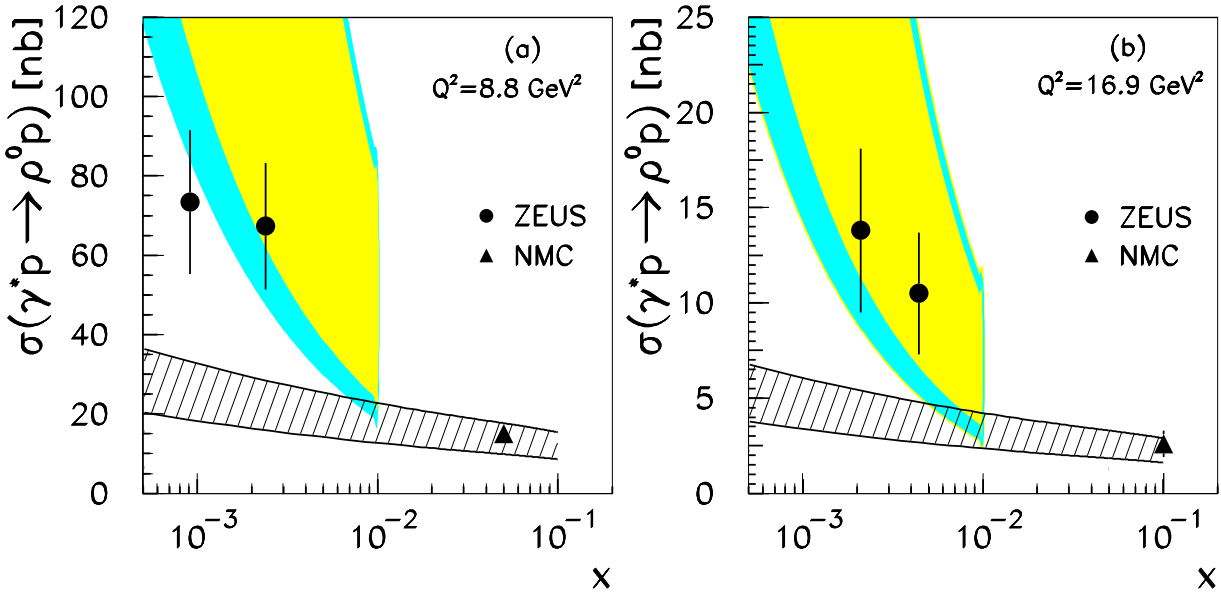
Figure 4: (a) The cross section, $\sigma(\gamma^* p \to \rho^0 p)$, as a function of x at a value of $Q^2 = 8.8$ GeV^2. (b) A similar plot for data at $Q^2 = 16.9$ GeV^2. The errors shown are only the statistical errors. In addition, there is a 31% systematic uncertainty which is not shown but applies to the overall normalisation. Also shown is the NMC result (which has an additional 20% normalisation uncertainty [7]). The shaded area corresponds to the predictions of Eqs. (3) and (11) for $x < 0.01$. The range of the predictions shown by the light shaded area is a result of the experimental uncertainty of the gluon distribution [18]. The dark shaded area includes the uncertainties on b and R added in quadrature to that of the gluon. In addition, there is a 50% uncertainty in the predicted cross section from the choice of the Q^2 scale; furthermore, the value of x in Eq. (3) is only defined to within a factor of 2. The hatched area displays the cross section expected from the soft pomeron model [11]. The range comes from the uncertainty in the measured value of b.